

# Interaction of Clouds, Radiation, and the Tropical Warm Pool Sea Surface Temperatures

*N. Schneider, G. J. Zhang, T. P. Barnett, and V. Ramanathan*  
*Scripps Institution of Oceanography*  
*La Jolla, California*

*U. Lohmann, and E. Roeckner*  
*Max-Planck-Institut für Meteorologie*  
*Hamburg, Germany*

## Introduction

The primary focus of this study is the Tropical Western Pacific (TWP). In this study, we combine in-situ observations (Tropical Ocean Global Atmosphere [TOGA]-Coupled Ocean Atmosphere Response Experiment [COARE] and Central Equatorial Pacific Experiment [CEPEX]) with satellite cloud data. Our objectives are fourfold:

- Use surface, aircraft and satellite observations to relate radiation fluxes within the atmosphere and at the surface to water vapor, clouds, cloud microphysical properties, and aerosols
- Use the observations to estimate the warm pool heat budget and the role of deep convection in regulating the evaporation and radiation fluxes at the sea surface
- Use the above results to develop and validate General Circulation Models (GCM) treatment of clouds, water vapor, radiation fluxes, and the surface heat budget over the TWP
- Use the GCM to understand the interactions between clouds, radiation, convection, and the TWP sea surface temperatures.

Recent results are presented on four interrelated issues: treatment of cloud-radiation interactions in GCMs, comparison between a GCM and observations of aspects of the moisture budget, the coupling between convection and surface evaporation, and penetrative radiation and its effect on TWP sea surface temperature (SST). These topics are relevant to the TWP radiation balance (Figure 1): clouds and atmospheric moisture influence the reflection and absorption of radiation; radiation and evaporation are both affected by convection and interact with TWP SST. Short wave radiation penetrates into the upper ocean

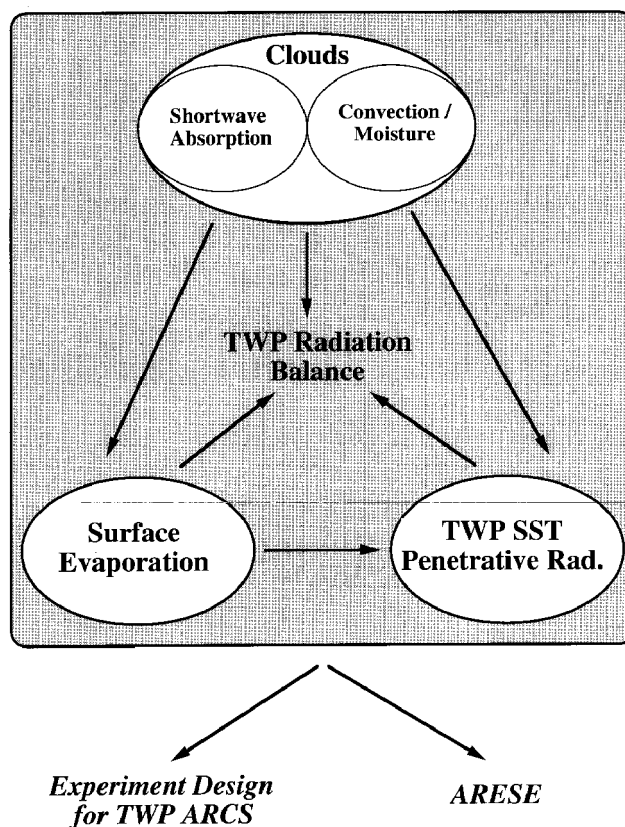


**Figure 1.** Conceptual relationships of studies presented in this report.

and, in combination with heat losses at the surface, can cause vertical mixing. Thus, it influences TWP SST and thereby the state of the overlying atmosphere. Finally, the results of our studies will help the experimental design of the TWP Atmospheric Radiation and Cloud Station (ARCS) and the upcoming ARM Enhanced Shortwave Experiment (ARESE).

## Treatment of Cloud-Radiation Interactions in GCMs

One of the fundamental objectives of our ARM related studies is to improve the treatment of cloud-radiation interactions in GCMs. Two recent ARM related studies (Cess et al. 1995 and Ramanathan et al. 1995) provide compelling evidence that the present generation of GCMs underestimate the absorption of solar radiation by clouds over the western Pacific warm pool by about  $35 \text{ Wm}^{-2}$ . We have begun a dedicated set of modeling and observational studies to track down the source of this serious deficiency and improve its treatment in GCMs.

*Excess Solar Absorption in TWP Cloud Systems.* To investigate the excess shortwave absorption by clouds, a numerical cloud generation model has been coupled to a discrete ordinates radiative transfer model (Lubin et al. 1995). The former was used to generate a cumulonimbus turret and three types of cirrus anvil (precipitating, extended, and detached) representing three stages of cloud evolution outward from the turret. The cloud particle size distributions, as a function of altitude, were used as input to the radiative transfer model using indices of refraction for pure water and pure ice, and equivalent sphere Mie theory. The radiative transfer model was used to calculate the ratio of cloud forcing at the surface to cloud forcing at the top of the atmosphere, both for the broadband shortwave and as a function of wavelength. Recent empirical studies have placed this cloud forcing ratio,  $f_s$ , at about 1.5, and our coupled model (Figure 2) easily yields this result for small solar zenith angles, when the cloud contains large ( $>20 \mu\text{m}$ ) ice particles that absorb significantly in the near infrared (primarily the 1.6 micron window). The model result underscores the importance of large particles in cloud-radiative interactions and uncovered a flaw of GCMs that neglect drop and ice particles  $>30 \mu\text{m}$ . However, the empirical studies are based on diurnal averages, and our plane-parallel radiative transfer model yields an area and diurnally averaged cloud forcing ratio of only 1.2 for a tropical cumulonimbus and cirrus anvil system, primarily because of the rapid decrease of the ratio with zenith angle. The ratio decreases because of the increase in albedo with zenith angle, which is a characteristic feature of plane parallel clouds. This study identifies one potential cause for underestimation of solar absorption by models: the neglect of realistic topography of cloud tops and cloud shapes may overestimate the reflection for slant zenith angles, which in turn reduces the solar radiation available for absorption within the interior of clouds. Adding dust or aerosol to the cloud layers, to make them absorb at visible wavelengths, makes this ratio even smaller because the solar zenith angle

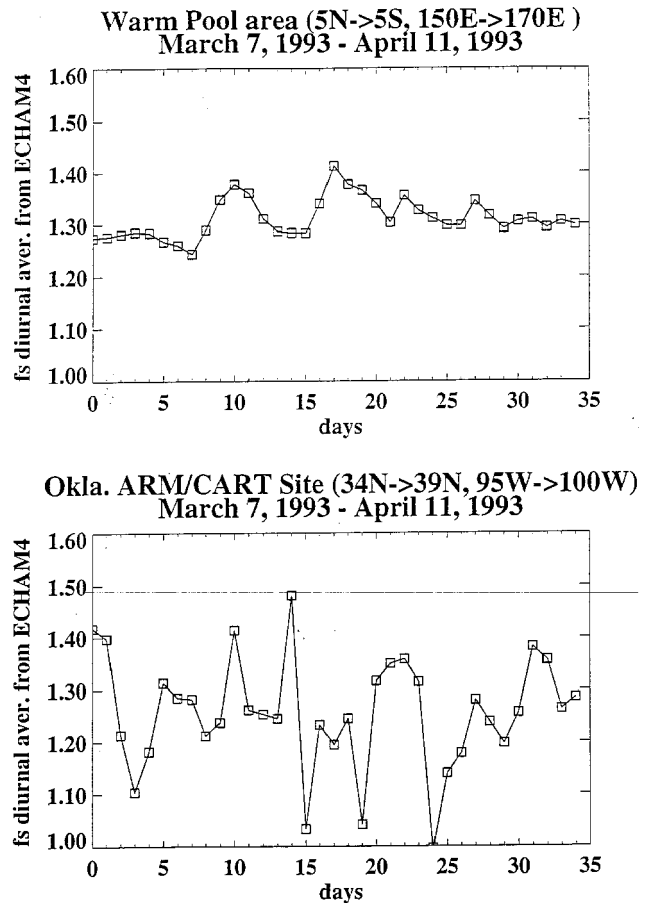


**Figure 2.** Time series of diurnally averaged cloud forcing ratio ( $f_s$ ) for TWP and Oklahoma ARM/CART sites from a simulation with ECHAM4.

dependence in the cloud forcing ratio becomes more pronounced in the presence of small absorbing particles. This study suggests that the ARESE experiment should focus on three issues: 1) the zenith angle dependence of cloud albedos; 2) the understanding of gaseous absorption throughout the near infrared, and 3) three-dimensional cloud effects.

*GCM Simulation Studies for the ARESE Experiment.* The objective of the ARESE experiment is to confirm excess absorption by direct observations and unravel the physics behind the excess absorption. The aircraft experiment will be conducted over Oklahoma in the fall of 1995. To design the sampling strategy, we have analyzed the geographical, synoptic and diurnal variations in  $f_s$ . Figure 3 compares the computed ratios for the Warm Pool with that for Oklahoma. The model reveals significant day-to-day fluctuations, and variation with cloud types and cloud altitudes (not shown).

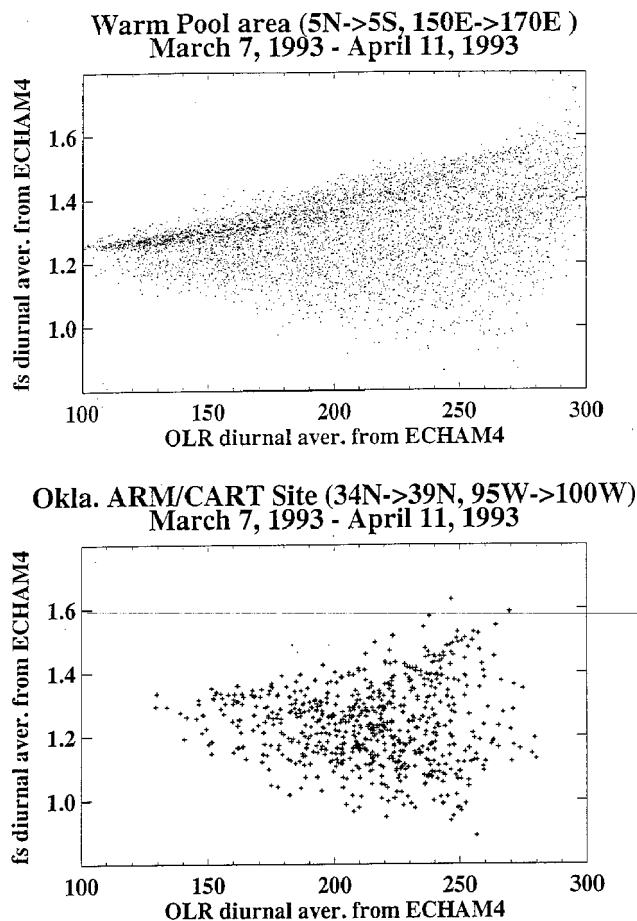


**Figure 3.** Scatter plot of diurnally averaged cloud forcing ratio ( $f_s$ ) versus OLR for TWP and Oklahoma ARM/CART sites from a simulation with ECHAM4.

The magnitude and temporal scale of the fluctuations suggest that an observational period of at least six weeks and preferably two months would be required. Also, the ratio in the model is significantly different between the two ARM sites (TWP and SGP). The GCM seems to suggest that we cannot generalize the Oklahoma findings and that the ARESE experiment should be repeated over the TWP.

## Comparison of Aspects of the Moisture Budget of ECHAM with CEPEX and Oklahoma ARM Site Measurement

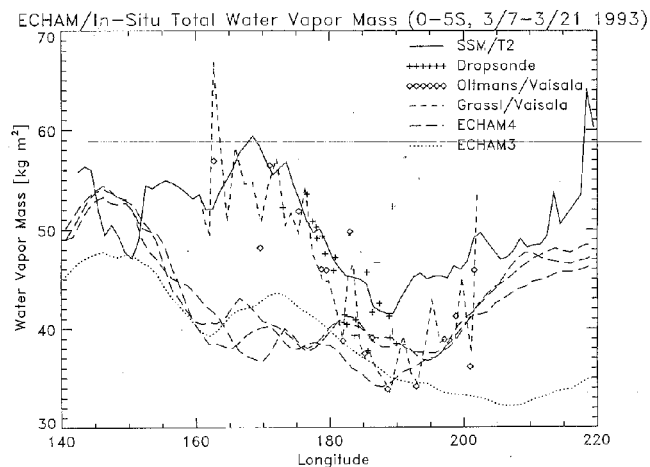
To demonstrate the use of observed data for GCM validation, aspects of the moisture budget are compared between

GCM simulations and field measurements taken during the CEPEX conducted from March 7 to April 5, 1993. One simulation of ECHAM3 and three simulations of ECHAM4 were carried out with slightly different initial conditions from the ECMWF analysis of March 1, 1993, and with the observed SST as lower boundary condition.

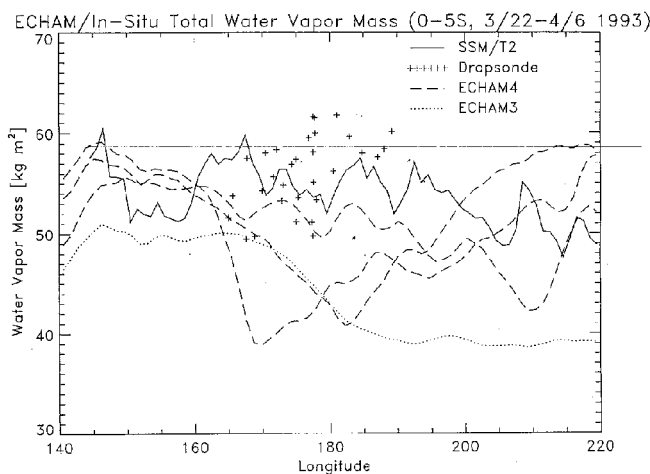
Radiosondes released between the equator and  $5^{\circ}\text{S}$  and the microwave satellite SSM/2 show a dry region east of the dateline in the first two weeks of CEPEX (Figure 4a), which vanishes in the second half of CEPEX (Figure 4b). ECHAM4 somewhat reproduces this change in convective activity, while ECHAM3 is too dry throughout and fails to pick up moisture in the second half in the eastern part. However, the three ECHAM4 simulations tend to develop different centers of convection later on, making comparison difficult.

Comparison of the mean relative humidity profiles indicates a dry bias in the mid troposphere and a moist one above 300 hPa, which shows up in ECHAM3, ECHAM4, and the ECMWF analyses (Figure 5). Microphysical cloud measurements conducted during CEPEX indicate an increase of ice water content (IWC) with temperature (McFarquhar and Heymsfield 1995). Its slope is similar but larger than data from a previous tropical dataset (Heymsfield 1993) indicate. While ECHAM3 systematically underestimates IWC, ECHAM4 results bear striking resemblance to the observations (Figure 6). Since many changes occurred from ECHAM3 to ECHAM4, such as new radiation code, detrained convective cloud water as a source for large scale water budget, and a change in the convection scheme, it is hard to determine what causes these differences.

To test the performance of ECHAM over land, a comparison was performed of the July/August total atmospheric water content above the Oklahoma ARM site from 8-day radiosonde measurements and the ECHAM3 (at T42 resolution) simulation (Figure 7). ECHAM3 was forced solely by global SSTs and was not initialized by observed atmospheric conditions. Thus, only the statistical properties of observations and simulation can be compared. It is impressive that the GCM simulated the correct mean water content over the month period. In addition, the simulated variability is reasonably close in magnitude and frequency to that observed, especially when it is realized that the comparison is between point observations and averaged properties of a GCM grid box (about  $250 \times 250$  [km<sup>2</sup>]).



a)



b)

**Figure 4.** East-west section of total water vapor mass. Total water vapor mass is derived from the Grassl and Oltmans upsondes situated on the Vickers R/V, dropsondes from the Learjet aircraft, the microwaver satellite SSM/2, ECHAM3 and ECHAM4 for the first a) and second half b) of CEPEX in the latitude belt 0-5°S.

## Coupling Between Convection and Evaporation

The TWP SST is governed by surface energy fluxes due to the relatively small ocean heat transport. Solar radiation and latent heat flux are the most important components; both are significantly affected by convection. While the effect of convection and its associated cloud systems on

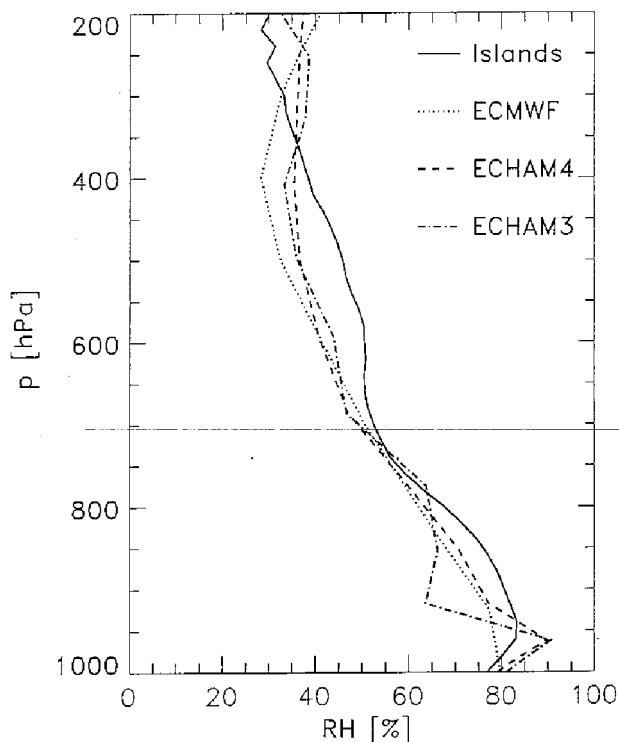


**Figure 5.** Mean relative humidity profiles. Mean relative humidity profiles averaged over the whole CEPEX time and domain from radiosondes released from all island stations, ECMWF analyses, ECHAM3 and ECHAM4.

reducing the surface solar radiation has been well recognized, the coupling of surface evaporation with convection and its associated circulation is not clear. Since convection is abundant in the warm pool, estimates of the role of surface evaporation in limiting the warm pool SST without considering the coupling between convection and surface evaporation could be in serious error. Thermodynamic theories predict that evaporation increases with SST, due to the exponential increase of surface saturation water vapor pressure with SST. However, the predictions are not supported by available observations.

Using the data collected from the Tropical Atmospheric Ocean (TAO) buoy array (Figure 8) deployed in the equatorial Pacific for the period from 1991 to 1993, we computed the surface evaporation and analyzed its relationship with SST (Zhang and McPhaden 1995). Figure 9 shows the surface evaporation as a function of SST binned at 1°K SST intervals. Also shown as functions of SST are the major factors contributing to surface evaporation, surface wind speed and surface saturation specific humidity deficit. For SST less than 301°K,

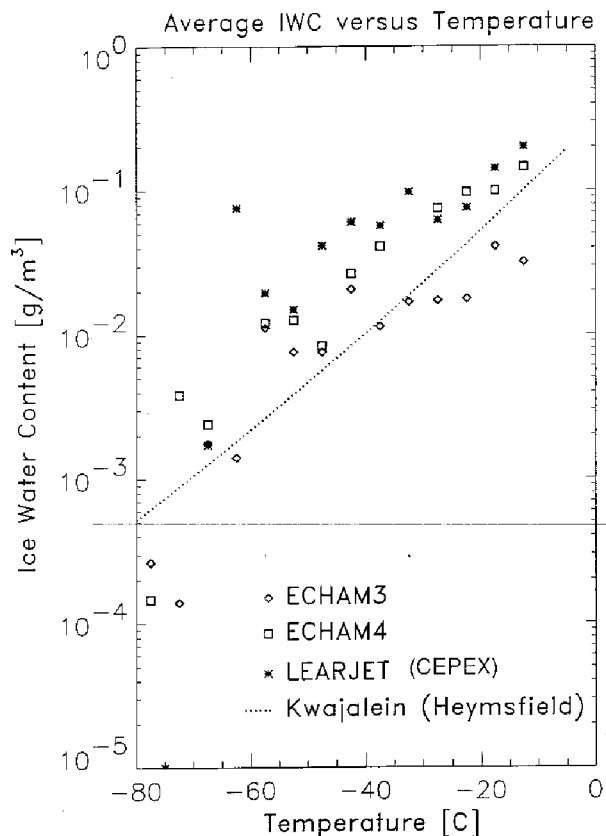


**Figure 6.** Ice water content (IWC) versus temperature. The average IWC for each 5 degree temperature bin versus temperature is derived from two-dimensional cloud probe data carried on the Aeromet Learjet (stars), ECHAM3 (rhombs) and ECHAM4 (squares). Additionally another derived relationship from a tropical dataset taken from the Kwajalein islands (Heymsfield 1993) is indicated as dashed line.

evaporation increases with SST as predicted by thermodynamic theories. However, after reaching a maximum of about  $110 \text{ Wm}^{-2}$  at SST close to  $301^\circ\text{K}$ , evaporation begins to decrease with SST. Comparison between wind speed and humidity deficit indicates that this is a result of the wind speed coupling with SST. Despite a fast increase of humidity deficit with SST, which tends to enhance evaporation at high SST, the strong decrease of winds with SST leads to decrease of evaporation with SST.

Why are surface winds coupled with SST? One likely process responsible for it is the interaction between convection and the large-scale low level circulation (Zhang et al. 1995). The frequency of convection has been found by many observational studies to strongly depend on SST statistically: below a threshold of about  $301^\circ\text{K}$ , little convection is found; above this threshold, the frequency

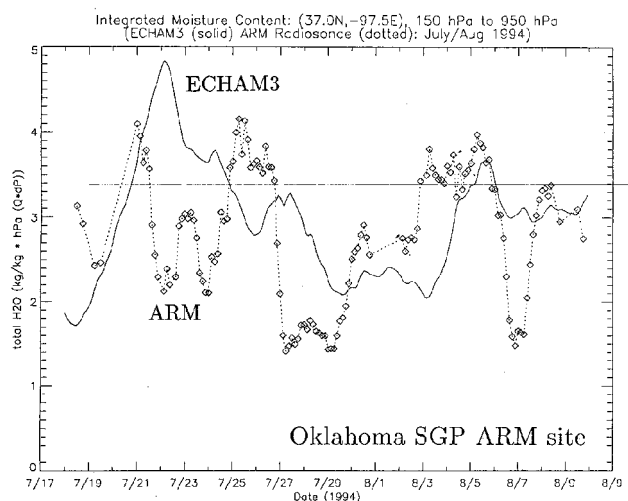


**Figure 7.** Comparison of the July/August total atmospheric water content above Oklahoma ARM site from 8-day radiosonde measurements (dotted) and the ECHAM3 AGCM at T42 resolution (solid).

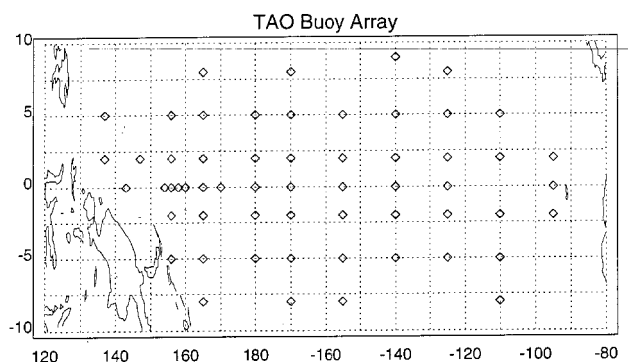


**Figure 8.** Positions of the TAO buoy array in the equatorial Pacific.

of convection increases sharply with SST (Graham and Barnett 1987, Neelin and Held 1987, Zhang 1993). Regions of convection are also regions of strong large-scale low-level mass convergence and weak surface winds. Figure 10 shows the cumulative frequency distribution of surface winds as a function of outgoing longwave radiation (OLR), a surrogate for convection, from the AVHRR satellite data. Clearly, low winds are observed much more frequently in convective regime (OLR less than  $240 \text{ Wm}^{-2}$ ) than in nonconvective regime. For instance, 50% of the observations have winds less than 4 m/s in convective regime, whereas only about 25% of the observations fall below this value in nonconvective regime.

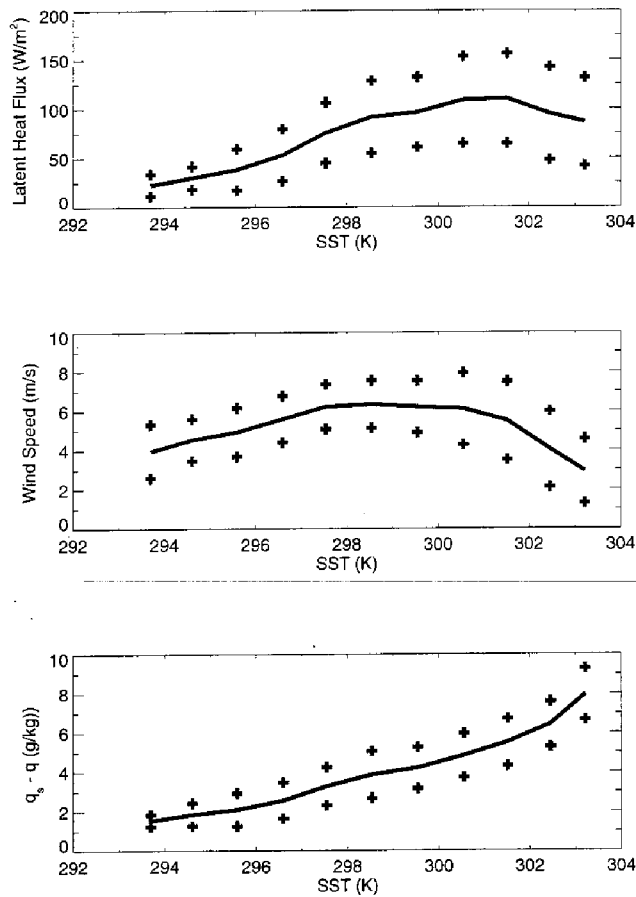


**Figure 9.** Surface evaporation, wind speed and air-sea humidity difference as functions of SST, as obtained from the buoy data. The means and the standard deviations for each SST bin are given.

In summary, contrary to common beliefs that surface evaporation should increase with SST, observations from the moored buoys show that for SSTs above  $301^{\circ}K$ , surface evaporation decreases with SST. This is a result of the sharp decrease of wind speed with SST, due to the coupling between convection and the low-level large-scale circulation. As SST increases above the threshold for the onset of convection, convection starts to develop. At the center of the large-scale low-level convergence that accompanies convection, wind speeds are low, resulting in lower surface evaporation.

## Penetrative Radiation

The analysis of TWP in a coupled ocean atmosphere model (Schneider et al. 1996) suggested that penetrative radiation not only deposits heat below the surface, but, in combination with heat losses at the surface, can destabilize

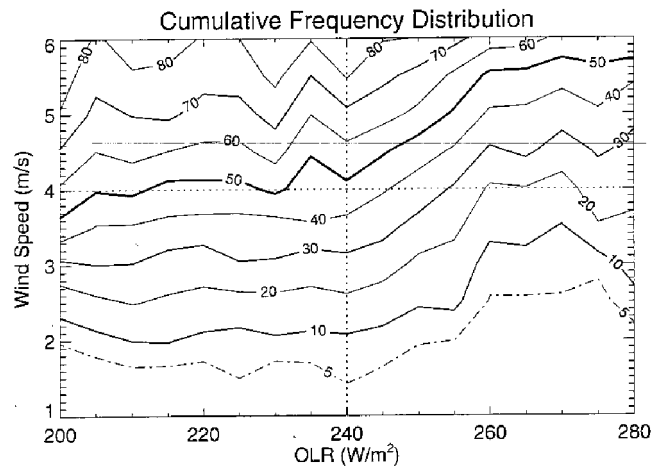


**Figure 10.** Cumulative frequency distribution of surface wind speed as a function of OLR (surrogate for convection) based on the two-year buoy data.

the water column and cause vertical mixing. Thus the partitioning of incident shortwave radiation and cooling due to radiation and turbulent heat fluxes exert significant control on the mixed layer depth, the surface heat budget of the ocean and planetary boundary layer and, ultimately, the processes of atmospheric convection and cloud formation.

Incident solar radiation at the surface of the ocean is partially absorbed below the surface of the ocean, while turbulent and radiative heat losses apply at surface. Thus the water column can be destabilized and vertical mixing can result. This mixing occurs as part of the diurnal cycle, where the large heat gains during the day are mostly removed at night. In regions of net heat gain, such as the tropics, this diurnal mixing is only possible with the penetrating part of the shortwave radiation heating the interior of the ocean. Without penetrative radiation, daytime heat gains at the surface exceed nighttime heat losses, and gravitational instabilities cannot develop.

The following simple model is a prototype for these physics and quantifies when the surface fluxes are conducive for night time mixing. Its application to TOGA COARE demonstrates the importance of penetrative radiation in controlling diurnal mixing and the evolution of surface temperatures.

Consider a one-dimensional model where the time rate of change of surface temperature and salinity are determined by the surface fluxes of heat and fresh water. The turbulent heat fluxes, long-wave radiation, and the fresh water flux apply at the surface of the ocean, and incident shortwave radiation is absorbed within the surface ocean

following a double exponential profile (Paulson and Simpson 1977). Mixing in the upper ocean occurs in response to static instability only and homogenizes the water column until it is gravitationally stable. Thus, convection is nonpenetrative, since the potential energy released during convection is dissipated rather than used to entrain waters from greater depths.

For the average surface fluxes of heat and fresh water observed during TOGA COARE ( $156^{\circ}\text{E}$ ,  $1^{\circ}45'\text{S}$ ), this model yields a mixed-layer depth of 36 m, surprisingly close to other estimates of the surface layer depth in the western Pacific. This is strong evidence that mixing induced by penetrative radiation and night time cooling can be as important as wind-induced mixing.

To further illustrate this point, Figure 11 shows the time evolution of SST from COARE mooring, and the solution to the model outlined above. The time period corresponds to October 22, 1992, to March 3, 1993. Despite the great simplicity of the model, and the complete lack of wind-induced mixing, the general SST tendencies are captured

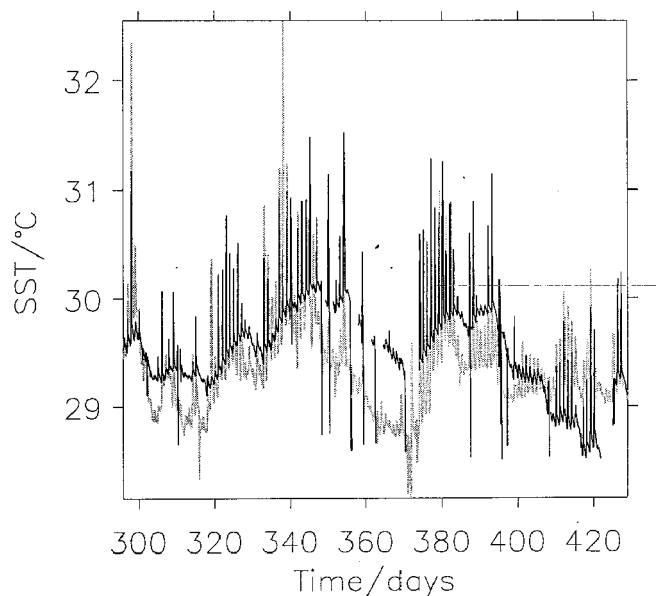


**Figure 11.** SSTs observed during TOGA COARE ( $156^{\circ}\text{E}$ ,  $1^{\circ}45'\text{S}$ ) from October 22 to March 3, 1993 (gray line), and sea surface temperatures predicted from a model that includes only surface fluxes of heat and fresh water, penetrative radiation, and non-penetrative convection (solid line). The model was forced by observed fluxes of heat and fresh water. Gaps in the simulated surface temperature correspond to very low surface temperatures associated with rain storms.

surprisingly well. The occasional short gaps in the simulation are due to very cool SSTs caused by heat losses and heavy precipitation that shut off nighttime mixing (Anderson et al. 1995). Largest differences between the simulation and observations are associated with strong winds, whose effect is not included in the model. The success of the simulation indicates that diurnal mixing due to penetrative radiation is a central mixing mechanism.

Neglect of penetrative radiation causes large errors in SST. Figure 12 shows observed, daily averaged SSTs, and those simulated by forcing a mixed layer model (Price et al. 1986) with surface fluxes observed during TOGA COARE. The model results with penetrative radiation reproduce the observed SSTs well, even though the one-dimensional mixed layer model underestimates the cooling during westerly wind burst. Disregard of the penetrative radiation yields a severe overestimation of surface temperatures by up to 3K during calm periods.

The importance of vertical mixing due to penetrative radiation that was hypothesized from a simulation with a coupled GCM was confirmed using observations. Thus, the relative magnitudes of incident radiation, and surface heat losses are of great importance for the heat budget of the ocean and planetary boundary layer and, ultimately, the processes of atmospheric convection and cloud formation.

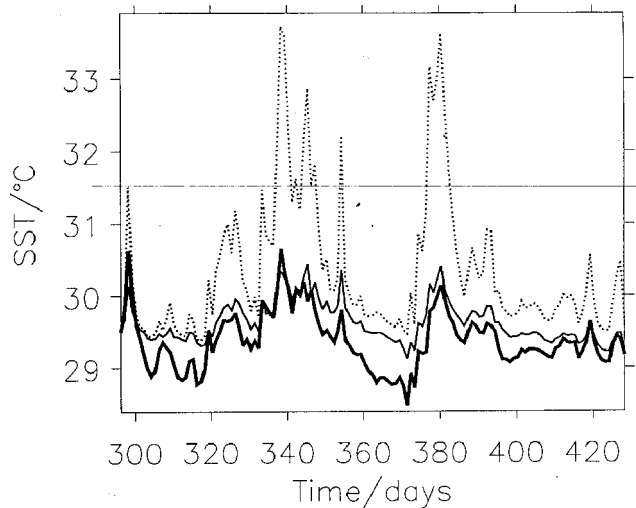


**Figure 12.** Daily averaged SSTs observed during TOGA COARE (solid thick line), simulated by a mixed-layer model (Price et al. 1986) with (solid thin line) and without (dotted line) penetrative radiation.

## Conclusion

The results presented here suggest that, to zeroth order, the warm pool SST is governed by surface heat budget and mixed-layer dynamics. Furthermore, the surface and atmospheric radiation fluxes are strongly regulated by deep convection and associated cloudiness. Thus, the TWP is an ideal natural laboratory to address issues related to clouds-radiation-climate feedback processes. We list here the primary conclusions from our study:

- We have a long way to go before successfully modeling the excess cloud absorption over TWP or SGP. However, our study uncovered two flaws in the treatment of clouds in GCMs: 1) The neglect of cloud drops or ice particles with size greater than about  $30\mu\text{m}$  (radius), a practice that tends to underestimate absorption; and 2) the plane parallel treatment of clouds tends to exaggerate the zenith angle dependence of cloud albedos, another reason for the underestimation of absorption in GCM clouds.
- Our GCM study suggests an observational period for ARESE experiment of at least six weeks and preferably two months.
- Comparison of observations of ECHAM3 and ECHAM4 and of observations from CEPEX and Oklahoma ARM site shows impressive simulations of aspects of the atmospheric moisture budget.
- Surface evaporation over TWP, where the annual mean SST is above  $301^\circ\text{K}$ , is strongly affected by deep convection through its interaction with the low level large-scale circulation. As a result, in the high SST and active convection regime, evaporation does not increase with SST, contrary to the predictions based on thermodynamic considerations alone.
- The importance of vertical mixing associated with penetrative radiation for TPW surface temperatures was confirmed using observations. Thus, the relative magnitudes of incident radiation and surface heat losses are of great importance for the heat budget of the TWP and planetary boundary layer and, ultimately, the processes of atmospheric convection and cloud formation.

We have used all available data to determine the long-term heat budget of the warm pool (Ramanathan et al. 1995). We need spatial and temporal variability of the radiation fluxes on a daily basis to relate the radiation fluxes to clouds, water vapor, and cloud microphysical properties. The three planned TWP ARCS stations along with 3-D analyzed fields will form the cornerstone of future study, which includes for the coming year:

- Use SGP radiation data in conjunction with ARESE data to unravel the physics behind the excess solar absorption.
- Use high spatial (Oklahoma) and high temporal (1 hour) resolution of GMS and GOES data to estimate the scale dependence of cloud radiation properties and develop a scale dependent cloud parameterization scheme for deep convective-cirrus clouds in TWP.
- Couple the convective parameterization with the cirrus cloud radiative parameterization in a GCM to unravel the role of convection and clouds and their associated physical, dynamical and radiative processes in the TWP heat budget.
- Investigate the coupling between convection, surface radiative heat flux, and evaporative cooling in interannual anomalies of the TWP using observations, atmospheric and coupled atmosphere-ocean circulation models.
- Investigate the dependence of the long-term average surface radiation and turbulent heat fluxes and SSTs on the specification of high-frequency (i.e., diurnal) forcing using a combination of an ocean mixed layer model and an atmospheric column model.

## Acknowledgments

This work is funded in its entirety by DOE ARM grant DOE DEFG 0391 ER 61198. We would like to thank Dr. D. Lubin for helpful discussion, Dr. M. McPhaden for use of the TOGA TAO data, the participants of CEPEX for providing invaluable measurements, Dr. D. Randall for soundings at the ARM Oklahoma SGP site, and Dr. R. Weller and the Woods Hole Oceanographic Institution for the use of TOGA COARE data.

## References

- Anderson, S. P., R. A. Weller and R. B. Lukas. 1995. Barrier layer formation in the western equatorial Pacific warm pool, *Nature*, accepted.
- Cess, R. D., M. H. Zhang, P. Minnis, L. Corsetti, E. G. Dutton, B. W. Forgan, D. P. Garber, W. L. Gates, J. J. Hack, E. F. Harrison, X. Jing, J. T. Kiehl, C. N. Long, J.-J. Morcrette, G. L. Potter, V. Ramanathan, B. Subasilar, C. H. Whitlock, D. F. Young, and Y. Zhou. 1995. Absorption of solar radiation by clouds: Observations versus models, *Science*, **267**, 496-499.

- Graham, N. E., and T. P. Barnett. 1987. Sea surface temperature surface wind divergence and convection over tropical oceans, *Science*, **238**, 657-659.
- Heymsfield, A. J. 1993. Microphysical structures of stratiform and cirrus clouds. In *Aerosol-cloud-climate interactions*, P. V. Hobbs (ed.), Academic Press, pp. 97-121.
- Lubin, D., J. P. Chen, P. Pilewskie, V. Ramanathan, and F. P. J. Valero. 1995. Microphysical examination of excess cloud absorption in the tropical atmosphere, *J. Geophys. Res.*, accepted.
- McFarquhar, G. M., and A. J. Heymsfield. 1995. In-situ observations of the horizontal and vertical structure of three cirrus anvils sampled during the Central Equatorial Pacific Experiment (CEPEX), *J. Atmos. Sci.*, accepted.
- Neelin, J. D., and I. M. Held. 1987. Modeling tropical convergence based on the moist static energy budget, *Mon. Wea. Rev.*, **115**, 3-12.
- Paulson and Simpson. 1977. Irradiance measurements in the upper ocean, *J. Phys. Oceanogr.*, **7**, 952-956.
- Price J. F., Weller R. A., and R. Pinkel. 1986. Diurnal cycling: observations and models of the upper ocean response to diurnal heating, cooling and wind mixing, *J. Geophys. Res.*, **91**, 8411-8427.
- Ramanathan, V., B. Subasilar, G. J. Zhang, W. Conant, R. Cess, J. Kiehl, H. Grassl, and L. Shi. 1995. Warm pool heat budget and shortwave cloud forcing: A missing physics? *Science*, **267**, 499-503.
- Schneider, N., T. B. Barnett, M. Latif, and T. Stockdale. 1996. Warm pool physics in a coupled GCM, *J. Climate*, **9**, 219-239..
- Zhang, C. 1993. Large-scale variability of atmospheric deep convection in relation to sea surface temperature in the tropics, *J. Climate*, **6**, 1898-1913.
- Zhang G. J., and M. J. McPhaden. 1995. The relationship between sea surface temperature and latent heat flux in the equatorial Pacific, *J. Climate*, **8**, 589-605.
- Zhang, G. J., V. Ramanathan, and M. J. McPhaden. 1995. Convection-evaporation feedback in the equatorial Pacific, *J. Climate*, **8**, 3040-3051.